Received: 5 July 2020 | Accepted: 10 November 2020

DOI: 10.1002/pamm.202000129

On the mechanical modeling of cell components

Sandra Klinge[1,*], **Tillmann Wiegold**[1], **Serhat Aygün**[1], **Robert P. Gilbert**[2], and **Gerhard A. Holzapfel**[3,4]

[1] TU Dortmund University, Institute of Mechanics, Leonhard-Euler-Str. 5, 44227 Dortmund, Germany
[2] University of Delaware, Department of Mathematical Sciences, 312 Ewing Hall, Newark, Delaware 19716, USA
[3] Graz University of Technology, Institute of Biomechanics, Stremayrgasse 16/2, 8010 Graz, Austria
[4] Norwegian University of Science and Technology (NTNU), Department of Structural Engineering 7491 Trondheim, Norway

Eukaryotic cells are complex systems which carry out a variety of different tasks. The current contribution gives insight into the modeling of some of their vital components and represents an overview of results achieved within the international D-A-CH project on computational modeling of transport processes in a cell. The first part of the contribution studies viscoelastic effects of cross-linked actin network embedded in cytosol. The basic-model is used to simulate the actin behavior at a microscopic level. It considers the influence of the physical length, the end-to-end distance and the stretch modulus in order to provide a relationship between the stretch of a single polymer chain and the applied tension force. The effective behavior of the cell cytoplasm is simulated by using the multiscale finite element method. Here, a standard large strain viscous approach is applied for the cytosol, while the generalized Maxwell model simulates viscous effects occurring in filaments due to deviatoric changes. The examples dealing with combinations of tension-holding tests give insight into the effective behavior of the cytoplasm.
The second part of the talk deals with the viral entry into a cell driven by the receptor motion. In the model developed, the receptor motion is described by the diffusion equation along with two boundary conditions. The first condition represents the balance of fluxes at the front of the contact area. To this end, the velocity is assumed to be proportional to the gradient of the chemical potential. The second condition deals with the energy balance and postulates that the difference in the energy behind and before the front causes the front's movement. The important energy contributions are energy due to the binding of receptors, the free energy of the membrane, the bending energy and the kinetic energy due to the motion of the receptors. The model yields a well-posed moving boundary problem, which is numerically solved using the finite difference method. The change of receptor density over the membrane as well as the motion of the front of the adhesion zone is studied in the numerical simulations.

1 Structure of the cytoplasm

Cytosol and cytoskeleton are two components of a cell which play an important role for its mechanical response. Cytosol is a gel-like material, whereas the cytoskeleton is a network, consisting of three types of elements: actin filaments, microtubules and intermediate filaments. The first part of the present contribution focuses on the study of the actin filament network embedded in the cytosol. Depending on its location, actin can comprise up to 10% of the cellular protein. A large amount of actin is present in the cells as globular monomer which polymerizes to filamentous actin. It is one of the proteins driving motility, protrusion and cell division. Being too stiff to form loops but flexible enough to exhibit thermal bending, actin filaments belong to the group of semi-flexible biopolymers.

2 Viscoelastic material model for the actin filament

The Holzapfel-Ogden β-model [1, 2] is assumed as the basis for the simulation of actin filaments. It provides a relationship between its arc-length L and its end-to-end distance r, i.e.

$$\frac{r}{L} = 1 + \alpha\, f^* - \frac{(1 + 2\,\alpha\, f^*)\,(1 + \alpha\, f^*)^{\beta}}{[1 + f^* + \alpha (f^*)^2]^{\beta}} \left(1 - \frac{r_0}{L}\right). \tag{1}$$

Here, r_0 denotes the end-to-end distance at zero force and the exponent β is addressed as the effective extensional modulus. The dimensionless stiffness $\alpha = \frac{\pi^2\, B_0}{\mu_0\, L^2}$ is expressed in terms of the stretch modulus μ_0 and the bending stiffness $B_0 = E\, I$, where E is the Young's modulus and I is the area moment of inertia. The dimensionless force is defined according to $f^* = \frac{f}{\alpha\, \mu_0}$. In this model, no explicit formulation for the potential of the external force is assumed. However, the derivatives $\Psi' = \Psi'(f^*)$ and $\Psi'' = \Psi''(f^*)$ of the potential can be calculated depending on the dimensionless force f^*, which is numerically calculated from Eq. (1).
Based on the previously described model, a new 2-node line element has been developed [1]. The position of an arbitrary point, belonging to such an element, is expressed as $\boldsymbol{X}^{\mathrm{e}} = \boldsymbol{X}^{\mathrm{e1}} + \tilde{\boldsymbol{X}}^{\mathrm{e}}\, \boldsymbol{R}$ in the reference configuration and as $\boldsymbol{x}^{\mathrm{e}} = \boldsymbol{x}^{\mathrm{e1}} + \tilde{\boldsymbol{x}}^{\mathrm{e}} \boldsymbol{t}$

* Corresponding author: e-mail sandra.klinge@tu-dortmund.de, phone +00 49 231 7555790, fax +00 49 231 7552688

in the current configuration. Here, $\boldsymbol{X}^{\mathrm{e1}}$, $\tilde{\boldsymbol{X}}^{\mathrm{e}}$ and $\boldsymbol{R}$ are the positions of the starting node, the distance from the starting node to the arbitrary point and the unit direction vector in the reference configuration, whereas $\boldsymbol{x}^{\mathrm{e1}}$, $\tilde{\boldsymbol{x}}^{\mathrm{e}}$ and $\boldsymbol{t}$ are the respective values in the current configuration. A special feature of the model chosen is that the deformation gradient $\boldsymbol{F}$ as well as the Cauchy stress tensor $\boldsymbol{\sigma}$ and the first and second Piola-Kirchhoff stress tensors $\boldsymbol{P}$, $\boldsymbol{S}$ are expressed depending on the corresponding scalar values and dyadic products of two direction vectors as follows

$$\boldsymbol{F} = \lambda\, \boldsymbol{t} \otimes \boldsymbol{R}, \quad \boldsymbol{\sigma} = \sigma\, \boldsymbol{t} \otimes \boldsymbol{t}, \quad \boldsymbol{P} = P\, \boldsymbol{t} \otimes \boldsymbol{R}, \quad \boldsymbol{S} = S\, \boldsymbol{R} \otimes \boldsymbol{R}, \tag{2}$$

where λ is the stretch and σ, P and S are scalar values which are functions of the derivative $\Psi'(f^*)$.
The second step of the FE-implementation is concerned with the formulation of the residual vector and the stiffness matrix. The common definition for the virtual internal work $\delta\Pi^{\mathrm{e}}_{\mathrm{int}} = \int_{V^{\mathrm{e}}} \boldsymbol{P} : \delta\boldsymbol{F}\mathrm{d}V$ is directly used to define the internal forces $\boldsymbol{f}^{\mathrm{e}A}_{\mathrm{int}} = \int_{V^{\mathrm{e}}} \boldsymbol{P} \cdot \nabla_{\boldsymbol{X}} N^A \mathrm{d}V$. Furthermore, the stiffness matrix is obtained from the derivative

$$\boldsymbol{K}^{\mathrm{e}AB}_{\mathrm{int}} = \frac{\mathrm{d}\boldsymbol{f}^{\mathrm{e}A}_{\mathrm{int}}}{\mathrm{d}\boldsymbol{x}^{\mathrm{e}B}} = 4\frac{A_{\mathrm{e}}}{L_{\mathrm{e}}}\frac{\partial P}{\partial \lambda}\frac{\partial N^A}{\partial \xi}\boldsymbol{t} \otimes \boldsymbol{t}\frac{\partial N^B}{\partial \xi} + 4\frac{A_{\mathrm{e}}}{l_{\mathrm{e}}}P\frac{\partial N^A}{\partial \xi}(\boldsymbol{I} - \boldsymbol{t} \otimes \boldsymbol{t})\frac{\partial N^B}{\partial \xi}. \tag{3}$$

The previous relationship depends on linear shape functions $N^A(\xi)$, A = 1,2, variable $\xi \in$ [-1,1], the element length in the current configuration l_{e}, the respective element length in the reference configuration L_{e} and the cross sectional area A_{e}. The general framework (Eq. (3)) is coupled to the material law (Eq. (1)) through the relationships $\Psi'_f = A_0\lambda_0 r_0 P$ and $\Psi''_f = A_0\lambda_0 r_0 \frac{\partial P}{\partial \lambda}$.
Finally, the model is enhanced by implementing viscous effects using the Maxwell model as the basis. According to this model, the non-equilibrium stress tensor $\boldsymbol{Q}^{\mathrm{v}}$ is introduced as an additional term. This term has the same structure as the second Piola-Kirchhoff tensor $\boldsymbol{Q}^{\mathrm{v}} = \tilde{Q}^{\mathrm{v}}\boldsymbol{R} \otimes \boldsymbol{R}$ such that the total stress reads

$$\tilde{\boldsymbol{S}} = \boldsymbol{S} + \boldsymbol{Q}^{\mathrm{v}} = \left(S + \tilde{Q}^{\mathrm{v}}\right)\boldsymbol{R} \otimes \boldsymbol{R} = \tilde{S}\boldsymbol{R} \otimes \boldsymbol{R}, \qquad \tilde{S} = \frac{\Psi'_f}{\lambda\lambda_0 A_0} + \tilde{Q}^{\mathrm{v}}. \tag{4}$$

The constitutive model is completed by coupling the evolution of the viscous part $\boldsymbol{Q}^{\mathrm{v}}$ to the evolution of the elastic stresses $\dot{\boldsymbol{Q}}^{\mathrm{v}} + \frac{\boldsymbol{Q}^{\mathrm{v}}}{\tau^{\mathrm{v}}} = \theta^{\mathrm{v}}\,\dot{\boldsymbol{S}}$, where τ^{v} is the relaxation time and θ^{v} the non-dimensional free-energy parameter.

3 Effective behavior of the cytoplasm

The application of the model is illustrated by a representative numerical example which is shown in Fig. **1** a). The multiscale finite element method (FEM) [3] is applied for this purpose. On the macroscopic level, a plate with dimensions of 100×100 µm is modeled. The representative volume element (RVE) has a square form with the side length 10×10 µm. The RVE includes 440 triangular elements simulating the cytosol and 668 line elements simulating the actin filaments. Material parameters of the cytosol are assumed as follows: $E_c = 20$ kPa, $\nu_c = 0.45$, $\tau_c = 2$ s and $\mu_c = 0.1$. Material parameters of the filaments are $\mu_0 = 38.6$ nN, $\lambda_0 = 1.027$, $\beta = 0.438$, $\alpha = 10^{-7}$, $\tau^{\mathrm{v}} = 2$ s and $\theta^{\mathrm{v}} = 0.835$.

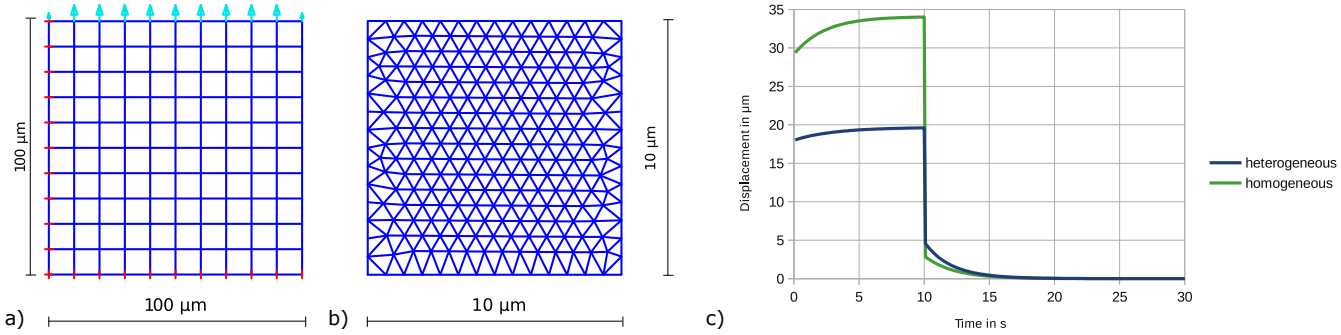

Fig. 1: a) Geometry and discretization of the plate. b) Geometry and discretization of the representative volume element. c) Deformation of the homogeneous cytosol compared to the deformation of the heterogeneous cytoplasm including the cytosol and actin filament network.

The upper edge of the macroscopic sample is firstly loaded by a constant distributed load of 5 kPa. In a second stage, the load is removed. Fig. 1 c) shows that the displacements grow and gradually achieve a stationary value during the loading stage. After the unloading, an elastic jump in displacements occurs and deformation gradually shrinks to zero. The same test is performed for a homogeneous material solely consisting of cytosol. A comparison shows that the displacements in the heterogeneous material are smaller than in the homogeneous material because of the strengthening effect of the filaments.

4 Numerical simulation of the viral entry into a cell

The second part of the present contribution focuses on the viral entry through the cells membrane. One of the main mechanisms used by viruses in order to enter a cell is receptor driven endocytosis [4]. During this process the virus connects its receptors to the receptors of the cell. This causes the cell membrane to bend and to build a vesicle around the virus. The process is characterized by the ability of the receptors of the cell to move freely within its membrane, while the receptors of the virus are fixed and occur with a much higher density. Upon contact, the virus dictates the required receptor density for bonding, thus causing the receptors of the cell to move towards the contact area. As a consequence, the contact area grows while the local receptor density of the cell changes, resulting in a moving boundary problem.

5 Endocytosis as a moving boundary problem

At the beginning of the process a virus connects to the cell and splits the cell membrane into two areas separated by an adhesion front. These two areas are characterized by the distribution of the receptor density $\xi(x,t)$. In the contact area the cell receptor density matches the constant receptor density of the virus $\xi(x,t) = \xi_{\text{eq}}$. In the area in front of the adhesion zone the density is a function of position and time $\xi(x,t)$ with its minimum at the adhesion front, where $\xi(x,t) = \xi_+$. Since the cell size is orders of magnitudes larger than the virus size, the density profile remains unchanged far away from the contact area $\lim_{x\to\infty} \xi(x,t) = \xi_0$. The motion of the receptors on the cell surface is based on the diffusion differential equation depending on the mobility m, i.e.

$$\frac{\partial \xi}{\partial t} = m \frac{\partial^2 \xi}{\partial x^2}. \tag{5}$$

A solution of this partial differential equation requires additional boundary conditions. The conservation of binders is considered first. It states that the amount of receptors required for the advancement of the adhesion front has to be equal to the amount of receptors provided by the flux. Following Fick's first law, the diffusion equation leads to the first boundary condition

$$(\xi_{\text{eq}} - \xi_+)\, v_+ - m \left[\frac{\partial \xi}{\partial x}\right]_+ = 0, \tag{6}$$

which depends on quantities related to the adhesion front [5]. Here, v_+ denotes the velocity of the front. For the second boundary condition an approach considering the energetic aspects of the front motion is chosen [6]. The front movement, represented by the kinetic energy $E_{\text{kin}} = \frac{1}{2}\, k\, T\, \xi_{\text{eq}}\, v_+^2$ is caused by the difference in the energy in front of and behind the front, each consisting of several contributions denoted by superscript "$-$" behind the front and superscript "$+$" in front of the front. Thus,

$$E_{\text{b}}^- + E_{\text{e}}^- + E_{\kappa}^- - E_{\text{e}}^+ + E_{\text{v}}^+ = E_{\text{kin}}. \tag{7}$$

Behind the front, $E_{\text{b}}^- = -k\, T\, C_{\text{b}}\, \xi_{\text{eq}}$ denotes a reduction in the free energy due to the binding of receptors, with k being the Boltzmann constant, T the absolute temperature and C_{b} a reduction factor. The term $E_{\text{e}}^- = k\, T\, \xi_{\text{eq}} \ln\left(\frac{\xi_{\text{eq}}}{\xi_0}\right)$ represents the energy associated with the entropy of receptors. Here, the initial binder density ξ_0 is adopted as a reference value. The term $E_{\kappa}^- = \frac{1}{2}\, k\, T B\, \kappa^2$ represents the energy related with bending, where κ is the curvature of the membrane and where B is the bending stiffness. In front of the front $E_{\text{e}}^+ = k\, T\, \xi_+ \ln\left(\frac{\xi_+}{\xi_0}\right)$ represents the energy associated with the entropy of receptors. The term $E_{\text{v}}^+ = \frac{1}{2}\, k\, T\, \xi_+\, v_{\text{r}}^2$ represents the kinetic energy of the receptors in front of the front moving towards the adhesion area, with v_{r} being their corresponding velocity. Finally, the second boundary condition is expressed in terms of the receptor density $\xi(x,t)$ and the front velocity v_+ by

$$\left[-\xi_{\text{eq}}\, C_{\text{b}} + \xi_{\text{eq}} \ln\left(\frac{\xi_{\text{eq}}}{\xi_0}\right) + \frac{1}{2} B \kappa^2\right] - \left[\xi_+ \ln\left(\frac{\xi_+}{\xi_0}\right) + \frac{1}{2}\, k\, T\, \xi_+\, v_{\text{r}}^2\right] = \left[\frac{1}{2}\, \xi_{\text{eq}}\, v_+^2\right]. \tag{8}$$

The corresponding non-linear system of equations is implemented by using the finite difference method and is solved numerically by a Newton Raphson scheme.

6 Numerical simulation of the virus uptake

The chosen numerical example simulates the uptake of a spherical virus treated as a 1D problem. The evolution of the receptor profile of the cell as well as the motion of the adhesion front are shown in Fig. 2. At the beginning of the process, the receptor density at the front experiences a strong decrease which weakens as the time progresses. The adhesion front advances

continuously during the whole process, while its velocity decreases towards a limit value. The numerical results are strongly influenced by the mobility parameter m which measures how fast the cell can provide receptors to the adhesion zone. Further important factors are the initial receptor density on the virus and on the cell membranes [6].

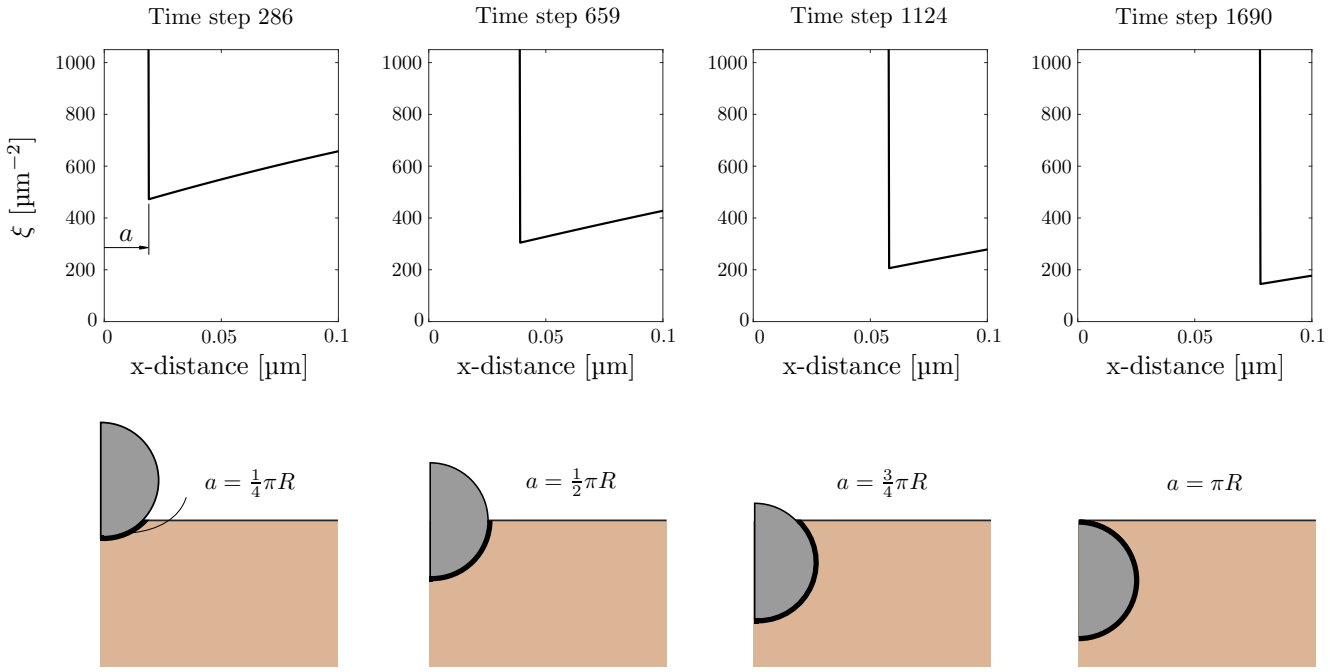

Fig. 2: Receptor density over the cell surface when the virus has entered the cell by 25%, 50%, 75% and 100%. Chosen process parameters are $m = 1\mu m^2/s$, $C_b = 5$, $B = 30$, $\xi_{eq} = 4800$ 1/µm^2, $\xi_+ = 1000$ 1/µm^2, virus diameter $D = 0.05\mu m$.

7 Conclusion

The first part of this contribution deals with the simulation of the effective behavior of the actin filament network embedded into cytosol. Attention is especially paid to the viscous effects which are introduced by the Maxwell model. The application of the model is illustrated by an example comparing the viscoelastic with the purely elastic behavior. The results show that the reinforcing effect of the actin filaments have a high impact on viscous effects compared to a homogeneous sample. A comprehensive comparison of the results with the experimental observation is envisaged as a topic of a future work. The second part of the present study focuses on the simulation of the influence of the binder mobility in the viral entry driven by receptor diffusion. The process is described by a diffusion differential equation accompanied by two boundary conditions. The two boundary conditions describe the flux balance and the energy balance at the adhesion front. The proposed moving boundary problem enables an efficient numerical simulation of the process and provides the basis for the consideration of additional relevant aspects. Bending of the cell in front of the adhesion front and an alternative expression for bending lipid bilayers are envisaged as topics of our future work.

Acknowledgements We gratefully acknowledge the financial support of the German Research Foundation (DFG), research grant No. KL 2678/7-1, and the Austrian Science Fund (FWF), research grant No. I 3431-N32.
Open access funding enabled and organized by Projekt DEAL.

References

[1] S. Klinge, S. Aygün, R. P. Gilbert and G. A. Holzapfel, Int. J. Num. Meth. Biomed. Eng., **34**(7), e2993 (2018).
[2] M. J. Unterberger, K. M. Schmoller, A. R. Bausch and G. A. Holzapfel, J. Mech. Behav. Biomed. Mater. **22**, 95-114 (2013).
[3] S. Klinge and K. Hackl, 2012, Int. J. Multiscale Comp. Eng. **10**(3), 213-227 (2012).
[4] M. M. Gibbons, T. Chou and M. R. D'Orsogna, J Phys Chem B **114**, 15403-15412 (2010).
[5] L. B. Freund and Y. Lin, J Mech Phys Solid **52**, 2455-2472 (2004).
[6] T. Wiegold, S. Klinge, R. P. Gilbert and G. A. Holzapfel, (submitted to Comput. Math. Appl.).

